Transmon qubit design for a cavity dimer in circuit QED

Lukas R. Heinzle

Semester thesis
Quantum Device Lab, ETH Zurich

Supervisor: Milan Allan
Prof. Andreas Wallraff

June 18, 2013

Abstract: Recent developments in superconducting circuits offer new possibilities for quantum simulation based on cavity quantum electrodynamics. For example one-dimensional arrays of coupled non-linear resonators allow to investigate interesting properties of phase transitions in quantum many-body systems. In this thesis I will describe the design of a superconducting "transmon" artificial two-level system for non-linear circuit QED resonator arrays. Based on electrostatic simulations, the resonator-transmon interaction is estimated and adjusted for a Dimer sample fabrication. Furthermore, the implementation of a potential *in-situ* tunable resonator-resonator coupling element is discussed.

Contents

Chapter 1

Introduction

Understanding correlated quantum many-body systems is one of the most challenging tasks in condensed matter physics. Although the fundamental interactions are often well known, the description of macroscopic systems is extremely difficult. Accessing the microscopic properties of such systems experimentally is very challenging due to the short time- and length scales involved. In 1966, Richard P. Feynman proposed to use well-controlled quantum systems in order to simulate strongly correlated large scale systems [Feynman82]. Following the ideas of Feynman, many applications to simulate complex quantum matter were developed theoretically, e.g. Refs. [Fisher89; Zohar13]. Experimental implementations of quantum simulators so far include cold atoms in optical lattices [Greiner02] and trapped ion systems [Barreiro11]. In recent years, new concepts for photon-based quantum simulators were proposed [Greentree06; Hartmann06]. The idea is to use coupled non-linear resonators in the context of cavity quantum electrodynamics (cavity QED) [Walther06]. Although photons in cavity QED systems have a bosonic nature, it is possible to simulate correlated fermionic problems with so called Bose-Hubbard models [Gersch62]. The Bose-Hubbard model is the bosonic counter part to the fermionic Hubbard model originated in solid-state systems [Hubbard63]. It describes the physics of interacting bosons in arrays or lattices and allows a mapping to the Hubbard model. The first experimental observation of quantum phase transitions with cold atoms [Greiner02] and entanglement generation [Romero-Isart07] makes the Bose-Hubbard model a cornerstone of quantum simulation with bosons. In the past years, solid-state versions of cavity QED systems became more and more popular. The ability to control macroscopic sized systems which behave quantum mechanically opens new possibilities. Especially circuit QED systems, where superconducting microwave resonators are coupled to artificial two-level systems [Wallraff04], seem to provide a interesting platform for quantum simulation [Houck12]. Therefore, I will now motivate quantum simulation with cavity QED systems. For simplicity, I limit myself to the description of one dimensional cavity arrays. Higher dimensional structures can be modeled by complex 2D lattices [Dimitris10; Schmidt12]

1.1 Quantum simulation with cavity QED systems

In cQED, a single mode of light in a resonator cavity can be described by a quantized harmonic oscillator Hamiltonian $H = \hbar\omega_0\hat{a}^\dagger\hat{a}$, where $\hbar$ denotes the reduced Planck constant, ω_0 the cavity resonance frequency and $\hat{a}^\dagger$ the photon creation operator obeying the bosonic commutation relation $[\hat{a}, \hat{a}^\dagger] = 1$. Implementations of such harmonic systems may be interesting for quantum information propagation [Plenio04]. For quantum simulation as discussed here, a sufficient anharmonicity in the energy level spectrum is required. The simplest configuration for such a non-linear cQED system is a single mode of light in a cavity interacting with a two-level system, also called quantum bit (qubit). By using dipole and rotating wave approximations, the interaction is described by the Jaynes-Cummings Hamiltonian

$$H_{JC} = \hbar\omega_0\hat{a}^\dagger\hat{a} + \frac{\hbar}{2}\omega_q\hat{\sigma}_z + \hbar g\left(\hat{a}^\dagger\hat{\sigma}^- + \hat{a}\hat{\sigma}^+\right), \tag{1.1}$$

where ω_q the two-level system transition frequency and g the coupling constant [Jaynes63]. Note that $\hat{\sigma}_z$, $\hat{\sigma}^\pm$ are the Pauli Spin - 1/2 notations for the ground state $|g\rangle$ and excited state $|e\rangle$ of the two level system, given by $\sigma_z = |e\rangle\langle e| - |g\rangle\langle g|$, $\hat{\sigma}^+ = |e\rangle\langle g|$ and $\hat{\sigma}^- = |g\rangle\langle e|$. As the Jaynes-Cummings model is one of the key elements in modern quantum optics, its applications are widely discussed [Walls94]. For resonant interactions between the resonator and qubit system, interesting bosonic quasiparticles, so called polariton modes are created by superposition of photon and qubit states [Yamamoto99].

The Jaynes-Cummings Hubbard model

By coupling many cavities (each with an on-site qubit) to a chain, a so called Jaynes-Cummings Hubbard model (JCHM) can be realized. The interplay between coupling and non-linearities from the individual cavities lead to interesting photon dynamics [Schmidt09]. The cavity array can be modeled by a superposition of the individual JC Hamiltonians and a nearest neighbor coupling J which gives

$$H_{JCHM} = \sum_{i=1}^{N} H_{JC,i} + J\sum_{i=1}^{N-1}\left(\hat{a}_i^\dagger\hat{a}_{i+1} + h.c.\right), \tag{1.2}$$

with the hermitian conjugate *h.c.* Potential applications for quantum simulation with JCHM arise for large cavity arrays [Hartmann08; Schmidt12]. Furthermore, such systems exhibit interesting polariton structures. In the limit of infinitely many cavities, the single Jaynes-Cummings polariton splitting evolves into a band structure [Nissen12].

The Bose-Hubbard model

As already mentioned, the basis for quantum simulation with bosonic systems is the Bose-Hubbard model. In principle, there are so called polaritonic and photonic Bose-Hubbard

systems which can be realize in cQED [Hartmann08]. The first systems are connected to the JCHM in the strong coupling regime, as the low energy polariton modes will form an effective Bose-Hubbard Hamiltonian [Leib10]. The derivation of such polariton models however is very involved and will not be discuss further. On the other hand, photonic Bose-Hubbard systems are conceptually simpler. For even stronger coupling between qubit and resonator, the cavity array exhibits strong non-linearities [Imamoğlu97]. This effect leads to either one or no photon in an individual cavity [Lang11]. In other words, the photons in the individual cavities can be treated as spin-1/2 fermions. The resulting Bose-Hubbard Hamiltonian reads

$$H = \hbar\omega_0 \sum_{i=1}^{N} \hat{a}_i^\dagger \hat{a}_i + \hbar\frac{U}{2} \sum_{i=1}^{N} \hat{a}_i^\dagger \hat{a}_i^\dagger \hat{a}_i \hat{a}_i + \hbar J \sum_{i=1}^{N-1} \left(\hat{a}_i^\dagger \hat{a}_{i+1} + h.c. \right), \tag{1.3}$$

where U denotes a Kerr non-linearity coefficient. Practical realizations of such a Bose-Hubbard Hamiltonian would allow to investigate interesting dynamics of correlated quantum many-body problems in condensed matter physics which are not accessible experimentally [Correa13].

1.2 Thesis outline

The aim of this semester thesis is to design transmon qubits for an existing coplanar microwave resonator array design [Korosec12]. This first chapter motivated quantum simulation with one-dimensional cavity arrays in cavity QED. Chapter two covers the framework for superconducting circuits with a review about microwave resonators and quantum bits (qubits) in superconducting circuits. Based on the theory, I will discuss the design of a transmon qubit in chapter three. A first step towards the implementation of a non-linear cavity array consists of realizing a "dimer" sample. The so called dimer sample consists of two coplanar microwave resonators coupled capacitively. Each resonator itself is coupled to a transmon qubit to obtain a non-linear behavior. In the fourth chapter I will propose an *in-situ* tunable resonator-resonator coupling element and discuss potential applications. The idea of this tunable coupler is to place a modified transmon design in between two resonators which mediates a dispersive coupling. Finally, I will conclude my semester thesis and give an outlook for observing "Majorana-like Modes of Light in a One-Dimensional Array of Nonlinear Cavities" [Bardyn12].

Chapter 2

QED in superconducting circuits

In this chapter I will introduce the theoretical framework for quantum electrodynamics in superconducting circuits (circuit QED). The first three sections summarize coplanar microwave resonators, superconducting qubits and their interaction. More detailed reviews for circuit QED can be found in [Devoret04a; Devoret07; Girvin09]. A final discussion about the relevant parameters for a two-cavity array (dimer) implementation concludes this chapter.

2.1 Coplanar waveguide resonators

The cavities considered in this thesis are realized as 1D coplanar waveguide (CPW) resonators in superconducting circuits [Göppl08]. Geometrically, a CPW is formed by a center conductor on a substrate, separated by a gap from the ground plane as shown in Fig. 2.1 (a) and (b). The waveguide characteristics are determined by the gap size, conductor and substrate properties [Gevorgian95]. A resonator is obtained by limiting the CPW to an optical length l, see Fig. 2.1 (c). The wavelength λ of the fundamental resonance mode is then given by $2l$. Other waveguides can be coupled capacitively to the resonator by a broad variety of coupling geometries.

In general, a CPW resonator can be modeled by a simple harmonic LC oscillator, where L represents the inductance and C the capacitance. The angular resonance frequency of the fundamental mode is $\omega_0 = 1/\sqrt{LC}$. Detailed discussions based on classical models can be found in [Pozar93]. A quantum mechanical treatment of such a CPW resonator is obtained by circuit quantization [Devoret97], in which the quantized conjugate variables are charge $\hat{q}$ and flux $\hat{\phi}$, obeying the commutation relation $[\hat{\phi}, \hat{q}] = i\hbar$. By re-expressing $\hat{q}$ and $\hat{\phi}$ with the bosonic creation- and annihilation operator $\hat{a}^\dagger$ and $\hat{a}$, the resonator Hamiltonian reduces to

$$H_{res} = \frac{\hat{q}^2}{2C} + \frac{\hat{\phi}^2}{2L} = \hbar\omega_0 \left(\hat{a}^\dagger \hat{a} + \frac{1}{2}\right), \tag{2.1}$$

where $Z_0 = \sqrt{L/C}$ the characteristic impedance and $\hat{a} = (\hat{\phi} + iZ\hat{q})/\sqrt{2\hbar Z}$ the bosonic annihilation operator. Based on the quantum mechanical treatment, the spectroscopic

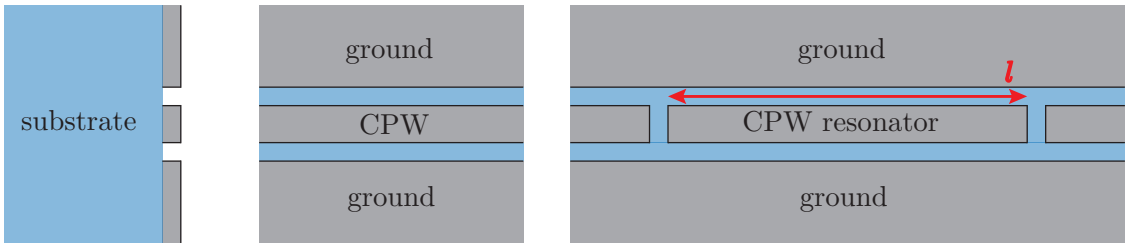

(a) (b) (c)

Figure 2.1: (a) Cross section of the CPW structure with the sapphire substrate (blue) and the Nb superconductor structures (gray). (b) Top view of the CPW structure. (c) CPW resonator of length l, capacitively coupled to two coplanar waveguides.

transmission can be calculated by using quantized Langevin equations and input-output theory [Walls94].

2.2 Artificial two-level systems

The physical realization of an artificial two level system requires non-linear elements in order to make the energy spectrum anharmonic. In superconducting circuits, non-dissipative Josephson junctions [Josephson62] provide a sufficient non-linearity. A schematic illustration of a Josephson junction is shown in Fig. 2.2 (a). Effective two-level systems based on Josephson junctions were initially developed in the context quantum computation [Makhlin01]. Usually, the ground state $|g\rangle$ and the first excited state $|e\rangle$ represent the two-level system. At low temperatures $k_B T \ll E_e - E_g$, where k_B is the Boltzmann constant and E_g the energy of state $|g\rangle$, the qubit will be thermally in its ground state. Microwave pulses applied to the resonator and qubit allow to manipulate and read-out the qubit state [Govenius12].

Cooper pair box

The most simplest realization of an artificial two-level system in superconducting circuits is the Cooper pair box (CPB) [Nakamura99]. The CPB qubit consists of two superconducting electrodes, coupled via Josephson junctions. Instead of using one Josephson junction, where the Josephson energy E_J is fixed, we will use the concept of a SQUID loop [Van Duzer81] which allows to tune E_J via the magnetic flux ϕ through the loop (Fig. 2.2 (b) according to

$$E_J(\phi) = E_{Jmax} \left| cos\left(\frac{\phi}{\pi\phi_0}\right)\right|, \tag{2.2}$$

where $\phi_0 = 2e/h$ is the magnetic flux quantum and E_{Jmax} the maximum Josephson energy determined by the junction properties [Fink10]. Thus it is possible to adjust the

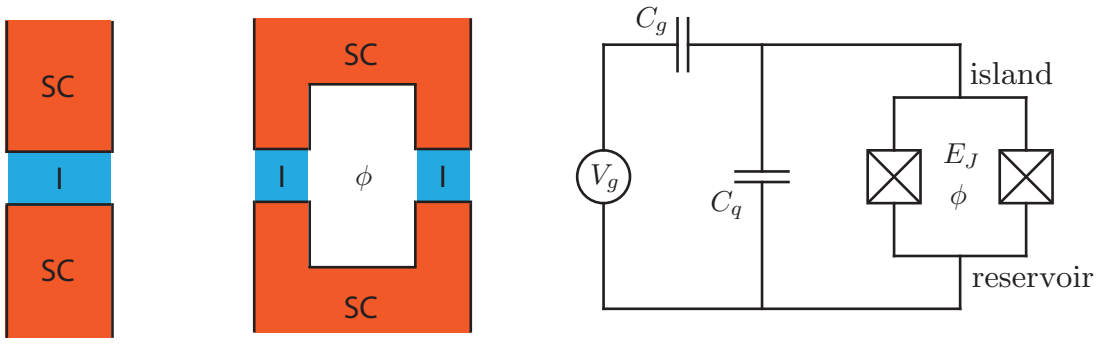

(a) (b) (c)

Figure 2.2: (a) Single Josephson junction. SL and I indicate the superconducting and insulating material, respectively. (b) A SQUID loop based on two Josephson junctions where ϕ denotes the flux through the junction area and sets the Josephson energy. (c) Effective schematic circuit for a voltage source V_g applied capacitively to a SQUID loop. The crossed boxes denote the Josephson junctions.

Josephson energy *in-situ* by using DC-biased coils [Göppl09]. The CPB Hamiltonian [Devoret04b] is given by

$$H = 4E_C(\hat{n} - n_g)^2 - E_J cos(\hat{\varphi}). \tag{2.3}$$

Here, $\hat{n}$ represents the number operator of Cooper pairs and $\hat{\phi}$ the gauge-invariant phase operator between the two electrodes called island and reservoir. The offset charge $n_g = Q_r/2e + C_g V_g/2e$ is composed of environmental charge on the island and the charge induced by applying an external voltage V_g capacitively to the SQUID loop as shown in Fig. 2.2 (c). The charging energy E_C required to add an additional electron from the voltage source V_g onto the island is

$$E_C = \frac{e^2}{2C_\Sigma}, \tag{2.4}$$

where $C_\Sigma = C_g + C_q$ is the total capacitance and C_q the SQUID loop capacitance. An improvement of the CPB is the so called transmon qubit, developed by Koch *et al.* [Koch07] which I will now discuss.

Transmon qubit

The major difference between the CPB and transmon is the Josephson to charging energy E_J/E_C ratio. The standard CPB works in a regime of $E_J/E_C \sim 1$, see Fig. 2.3 (a), whereas for the transmon qubit $E_J/E_C \gg 1$ holds. The energy level diagram is then similar to Fig. 2.3 (c), where the individual energies E_m obtained by second order perturbation theory are

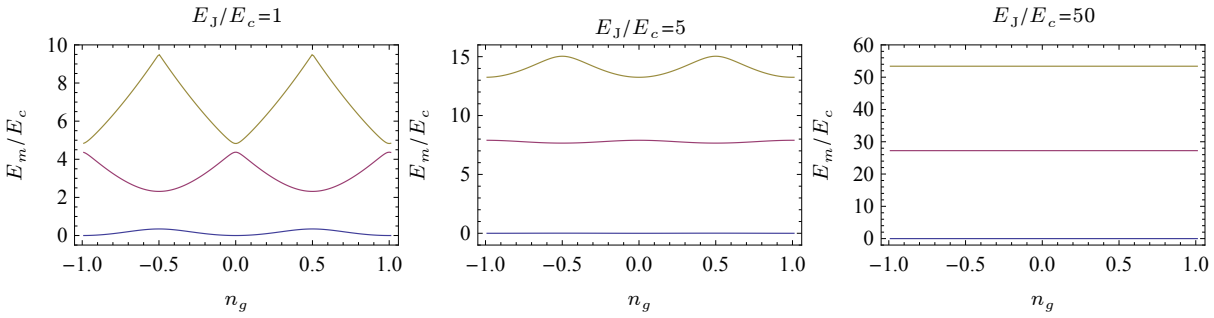

Figure 2.3: Energy leves of the CPB design for (a) $E_J/E_C = 1$, (b) $E_J/E_C = 5$ and (c) $E_J/E_C = 50$. The Transmon qubit is designed to work in the regime of (c).

$$E_m \approx -E_J + \sqrt{8E_C E_J}\left(m + \frac{1}{2}\right) - \frac{E_C}{12}\left(6m^2 + 6m + 3\right). \tag{2.5}$$

The charge sensitivity $\epsilon_m \equiv E_m(n_g = 1/2) - E_m(n_g = 0)$ of the energy levels E_m is given by

$$\epsilon_m \sim e^{-\sqrt{8E_J/E_c}}. \tag{2.6}$$

Thus, for typical transmon designs with $E_J/E_C \gg 1$, the sensitivity to charge noise n_g is reduced significantly compared to the standard CPB. This charge insensitivity results in a reduced anharmonicity. The energy difference between the ground state $|g\rangle$ and the first excited state $|e\rangle$ is given by $E_{ge} = E_e - E_g = \hbar\omega_q$ which leads to

$$\hbar\omega_q = \sqrt{8E_J E_C} - E_C \tag{2.7}$$

2.3 Resonator - qubit coupling

By coupling a CPB or transmon qubit to a CPW resonator, solid state cavity QED systems are realized [Wallraff04]. This interaction can be descirbed by the celebrated Jaynes-Cummings model [Jaynes63]. In other words, the resonator - transmon coupling can be approximated by dipole interaction [Blais04]. To study the interaction between the transmon qubit and the resonator, we start with an effective Hamiltonian resulting from circuit quantization:

$$H = 4E_C(\hat{\hat{n}} - n_g)^2 - E_J cos(\hat{\varphi}) + \hbar\omega_0 \hat{a}^\dagger \hat{a} + 2\beta e V^0_{rms} \hat{n}\left(\hat{a} + \hat{a}^\dagger\right) \tag{2.8}$$

The first and second term correspond to the transmon and resonator Hamiltonian, whereas the third term represents the interaction. Re-writing equation (2.8) in the basis of uncoupled transmon eigenstates $|i\rangle$ gives

$$H = \hbar\omega_0 \hat{a}^\dagger \hat{a} + \sum_i E_i |i\rangle\langle i| + \hbar \sum_{i,j} g_{ij} |i\rangle\langle j| \left(\hat{a} + \hat{a}^\dagger\right). \tag{2.9}$$

with coupling energies $\hbar g_{ij} = \hbar g_{ij}^* = 2\beta e V_{rms}^0 \langle i|\hat{n}|j\rangle$. The root-mean-square voltage of the local oscillator is $V_{rms}^0 = \omega_0\sqrt{\hbar Z_0/\pi}$ with $Z_0 = 50\Omega$. The parameter $\beta = C_g/C_\Sigma$ is defined as the ratio between gate and total capacitance. For typical transmon designs with $E_J/E_C \gg 1$, only the nearest neighbor coupling ($i = j \pm 1$) in the matrix element $\langle i|\hat{n}|j\rangle$ is relevant. The perturbative approach to calculate the nearest neighbor matrix elements is shown in appendix C of [Koch07] and gives

$$|\langle j+1|\hat{n}|j\rangle| \approx \sqrt{\frac{j+1}{2}}\left(\frac{E_J}{8E_C}\right)^{1/4} \tag{2.10}$$

With a rotating wave approximation (RWA) it is possible to eliminate more terms of equation (2.9) which yields to

$$H = \hbar\omega_0\hat{a}^\dagger\hat{a} + \sum_i E_i|i\rangle\langle i| + \hbar\sum_i g_{i,i+1}\left(|i+1\rangle\langle i|\hat{a} + |i\rangle\langle i+1|\hat{a}^\dagger\right). \tag{2.11}$$

Finally, by using the Pauli Spin-1/2 notation $\sigma_z = |e\rangle\langle e| - |g\rangle\langle g|$, $\sigma_+ = |e\rangle\langle g|$ and $\sigma_- = |g\rangle\langle e|$ we can re-write the effective Hamiltonian in the well known Jaynes-Cummings form

$$H = \hbar\omega_0\hat{a}^\dagger\hat{a} + \frac{\hbar}{2}\omega_q\sigma_z + \hbar g\left(\hat{a}^\dagger\sigma_- + \hat{a}\sigma_+\right), \tag{2.12}$$

with coupling energies

$$\hbar g \equiv \hbar g_{01} \approx 2e\beta\omega_0\sqrt{\frac{\hbar Z_0}{\pi}}\left(\frac{E_J}{8E_C}\right)^{1/4}. \tag{2.13}$$

2.4 Towards cavity arrays in circuit QED

Now that the individual elements required for an experimental implementation of coupled cavity arrays are now introduced, it is time do discuss the relevant scales of the coupling rates. The Jaynes-Cumming Hubbard and Bose-Hubbard model for quantum simulation motivated in the introduction both require to work in the strong coupling regime [Wallraff04] with large cooperativity factors ξ, defined by

$$\xi \equiv \frac{g^2}{2\kappa\gamma} \gg 1, \tag{2.14}$$

where κ denotes the resonator decay rate and a γ spontaneous qubit decay rate due to dissipation [Ithier05; Göppl08]. The initial work of designing a dimer cavity array was done by [Korosec12]. The fundamental resonance frequency of the individual cavities is set to be $\omega_0/2\pi = 7\,\mathrm{GHz}$. By adjusting the capacitive coupling between the CPW resonators and the open CPW transmission lines, the resonator decay rate was set to $\kappa = 1\,\mathrm{MHz}$ and the capacitive resonator-resonator coupling to $J/2\pi = 30\,\mathrm{MHz}$. Current circuit QED setups in the QUDEV lab at ETH Zurich [Steffen13] can achieve transmon qubit decay rates with an upper bound of $\gamma/2\pi \leq 1\,\mathrm{MHz}$. This leaves the discussion up to specify

the resonator-qubit coupling g. In order to realize polaritonic or photonic Bose-Hubbard models, the coupling strength is intended to be $g/2\pi \sim 130\,\mathrm{MHz}$ at $E_J(\phi) = E_{Jmax}$. Thus, g is tunable by changing the flux through the SQUID loop from $0 \leq g \leq 130\,\mathrm{MHz}$. This set of parameters g, κ, γ allows us to adjust $0.2 \leq g/J \leq 4.3$ while keeping the strong coupling regime $18 \leq g^2/2\kappa\gamma \leq 8450$. The polaritonic Bose-Hubbard model can be realized for $\xi \sim 10^2$ whereas the photonic Hubbard model requires $\xi \sim 10^3 - 10^4$ [Leib10]. Although ξ can be varied over a large range, the ratio g/J significantly changes. Therefore, it is desirable to have *in-situ* tunable J. A possible implementation scheme of such a tunable resonator-resonator coupling is discussed in chapter 4.

Chapter 3

Transmon qubit design

A crucial element for quantum simulation with coupled cavity arrays are non-linear elements. In circuit QED, this non-linearity is introduced by coupling a CPW resonator to an artificial two-level system (transmon qubit) which allows to reach the strong coupling regime [Wallraff04; Lang11]. In this chapter, I will focus on the transmon qubit design and estimate the resonator-qubit coupling from electrostatic simulations. One goal of the new transmon design are improved coherence times. To demonstrate the transmon properties experimentally, a dimer sample was fabricated.

3.1 Design outline

The target is to design a transmon qubit with a coupling rate of $g \sim 130\,\mathrm{MHz}$ as discussed in section 2.4. For the first experiments with a dimer sample, a charging energy of $E_C/h = 300\,\mathrm{MHz}$, where h is Planck's constant is intended. Furthermore, high qubit coherence times are desired to keep the spontaneous qubit decay rate γ below $1\,\mathrm{MHz}$. Recent experiments in the *Quantum Device Lab* at ETH Zurich used large transmon design patterns to achieve qubit coherence times of up to $2\,\mu\mathrm{s}$ [Steffen13]. It is believed that these coherence times are mainly limited by the small gaps between the resonator and qubit electrodes. For similar transmon qubit designs with much larger gaps, coherence times of up to $9\,\mu\mathrm{s}$ were reached [Chow12]. Thus, the idea behind the design in this semester thesis is to use larger gaps between all the individual superconducting elements [Chang13]. Moreover, I try to locally minimize the electric field strengths by using rounded edges.

The maximum size of the transmon qubit is $150\,\mu\mathrm{m} \times 350\,\mu\mathrm{m}$, given by the resonator mask [Korosec12]. The resulting qubit design with the geometric properties is shown in Fig. 3.1. The next section describes how the transmon coupling rate g and charging energy E_C can be estimated based on electrostatic simulations. Intuitive instructions how to modify the design towards desired g and E_C values can be found in [Burkhard12].

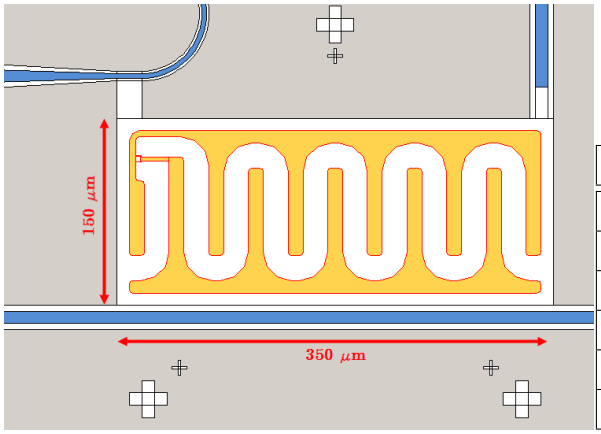

(a)

Parameter	Value
Finger width	12 μm
Finger length	95.2 μm
Finger spacing	19.8 μm
Ground / resonator spacing	10 μm
Fillet radius	3 μm
SQUID size	4 μm× 5 μm

(b)

Figure 3.1: (a) Design of the transmon qubit electrodes (yellow) with the resonator-, charge- and fluxline (blue). (b) Geometric properties of the transmon qubit.

3.2 Electrostatic simulation

The electrostatic environment of the transmon is essential for g and E_C according to Eqs. (2.13) and (2.4), respectively. The complete capacitive environment [Koch07] can be approximated as an effective capacitance network shown in Fig. 3.2. Based on this model which contains the relevant capacitances, the total capacitance C_Σ which the qubit experiences is given by

$$C_\Sigma = \frac{(C_{12}+C_{24})(C_{13}+C_{14})}{C_{12}+C_{13}+C_{24}+C_{34}} + C_{23} + C_J, \tag{3.1}$$

where the qubit capacitance C_J is assumed to be 6 fF. The geometric factor in the coupling rate is given by the capacitance ratio

$$\beta = \frac{C_{12}C_{34} - C_{13}C_{24}}{(C_{12}+C_{24})(C_{13}+C_{34}) + (C_{12}+C_{13}+C_{24}+C_{34})(C_{23}+C_J)}. \tag{3.2}$$

derived in [Burkhard12]. Electrostatic simulations with *Ansoft Maxwell 14* resulted in a total capacitance of $C_\Sigma = 67.22\,\text{fF}$ and a capacitance ratio of $\beta = 0.122$. By assuming a resonator frequency of $\omega_0/2\pi = 7\,\text{GHz}$ and a maximum Josephson energy of $E_J/h = 30\,\text{GHz}$ from the SQUID loop design and fabrication process, it is possible to evaluate the resonator-qubit coupling g and the qubit charging energy E_C with Eqs. (2.13) and (2.4) as summarized in Tab. 3.1.

	Specification	Simulation
g	130 MHz	127 MHz
E_C	300 MHz	290 MHz

Table 3.1: Electrostatic simulation results for the transmon-resonator coupling rate g and the charging energy E_C

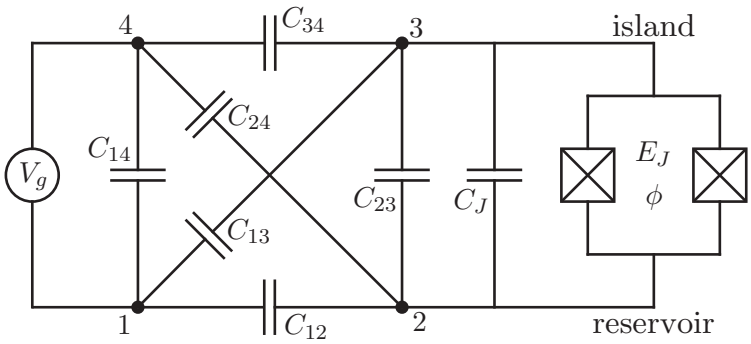

Figure 3.2: (a) Reduced capacitive environment for a transmon qubit [Koch07]. C_J denotes the intrinsic capacitance of the Josephson SQUID loop.

3.3 Dimer fabrication

In order to investigate the properties of the designed transmon experimentally, a dimer sample including transmon qubits was fabricated in the *FIRST* cleanroom at ETH Zurich, see Fig. 3.3. I will now shortly summarize the fabrication process [Fink10]. First, the microwave coplanar waveguide resonator structures with feature sizes in the micrometer range are realized with photo-lithography techniques. Therefore a 4-inch sapphire wafer, sputtered with a 75 nm niobium (Nb) layer is coated with a photo resistive material. The photo-lithography mask aligned to the waver is then illuminated with UV light. All areas exposed the the UV light are finally removed by chemical developing.

In the second process step, the transmon qubit electrodes and Josephson junctions for the SQUID are deposited on the microchip. Since the Josephson junctions have much smaller feature sizes of the order of a few nanometers, it is not possible to apply the same photo-lithography techniques as for the CPW resonators. Instead, the Transmon qubits are processed by an electron beam lithography (EBL). A special bilayer resist for EBL is deposited on the sample which already contains the Nb resonator structures. With an additional PMMA layer baked at 180 °C, the electron beam can write the designed qubit mask onto the microchip. By depositing aluminum, letting it oxidize for a certain time, and again depositing aluminum, the Josephson junctions are fabricated [Fink10]. As a last step, the resist is removed and the microchip is bonded to a printed circuit board (PCB). The PCB contains connectors for superconducting cables, compatible to the experimental setup of the cryogenic dilution refrigerator [Schmidlin08].

Unfortunately, the Dimer sample fabricated did not work as it was cooled down and tested in the dilution refrigerator. We think that the Josephson junctions are not working properly since spectroscopy measurements indicate only a resonator splitting similar to dip-stick sample tests [Karalic13]. Thus I cannot show any interesting measurement results concerning transmon coupling rates or coherence time improvements.

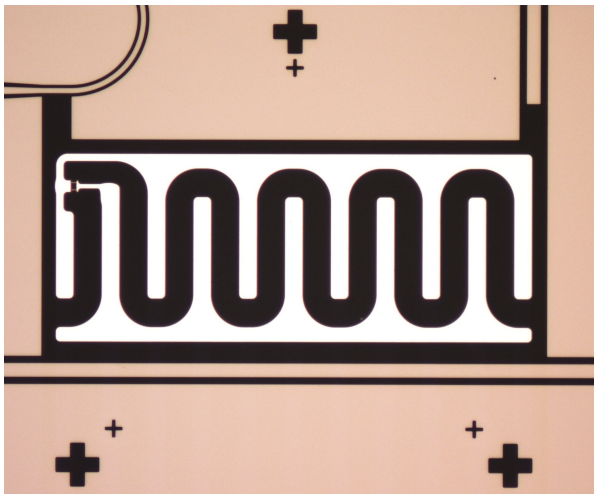

Figure 3.3: Microscope image of the fabricated transmon qubit. The bright colored elements are the qubit electrodes (Al)

Chapter 4

Proposal: Tunable resonator-resonator coupling element

For capacitively coupled cavity arrays, the coupling rate J between the individual resonators is fixed. For realizing a polaritonic or bosonic Bose-Hubbard model, it is often useful to adjust the coupling *in-situ* [Nissen12]. If an ideal two-level system (qubit) is placed inbetween two cavities, an additional "quantum" coupling arises [Johnson11]. The proposal of this chapter is to place a modified transmom design inbetween two CPW resonators. This approach is similar to suggested flux qubits for tunable coupling elements in circuit QED [Mariantoni08]. Electrostatic simulations similar to section 3.2 are used for a priori estimations of the relevant coupling rates. Implementing such a tunable coupling element allows interesting applications like e.g. new qubit readout schemes [Sete13]. I will start with reviewing the general theory for a two-level mediated cavity-cavity coupling.

4.1 Two cavity architecture

The aim of this section is to describe the dispersive coupling mediated by a two-level system between two cavities [Johnson11]. For simplicity, the two cavities are assumed to have equal resonance frequencies ω_0. We can start with the Jaynes-Cummings Hamiltonian of the two individual resonators and consider a direct coupling J_0 between the two resonators, see Fig. 4.1. This yields a Hamiltonian

$$H = \hbar\omega_0 \sum_{i=1}^{2} a_i^\dagger a_i + \frac{\hbar}{2}\omega_q \sigma_z + \sum_{i=1}^{2} \hbar g_i \left(a_i \sigma^+ - a_i^\dagger \sigma^- \right) + \hbar J_0 \left(a_1^\dagger a_2 + a_2^\dagger a_1 \right), \tag{4.1}$$

where ω_q is the qubit transition frequency and $g_{1,2}$ cavity-qubit coupling rates. In the dispersive regime,where the coupling coefficients $g_{1,2}$ are small compared to the cavity-qubit detuning $\Delta = \omega_q - \omega_0$, i.e. $g_{1,2}/\Delta \ll 1$, the effective Hamiltonian can be obtained by a Schrieffer-Wolff method [Bravy11]. The procedure is similar to the dispersive limit

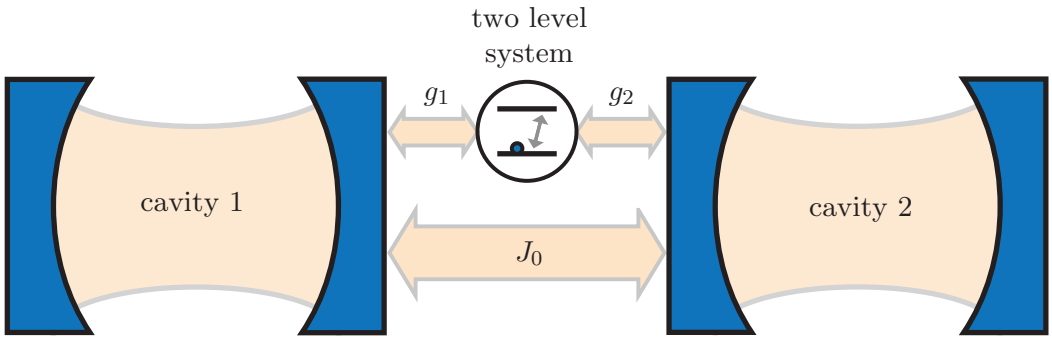

Figure 4.1: Schematic of the two-cavity architecture. Both cavities are coupled to one two-level system by g_1 and g_2, respectively. The direct nearest neighbor coupling rate is denoted by J_0.

for one cavity-qubit system [Blais04]. The unitary operator $\hat{U}$ can be written as

$$\hat{U} = exp\left[\sum_i \frac{g_i}{\Delta_i}\left(a_i\sigma^+ - a_i^\dagger\sigma^-\right)\right], \tag{4.2}$$

and the effective Hamiltonian is then given by a transformation $H' = U^\dagger H U$. For the dispersive regime where $g_{1,2}/\Delta \ll 1$ holds, it is possible to approximate H' by a series expansion up to coefficients of order $g_{1,2}^2/\Delta^2$ by using the Barker Campbell Hausdorff relation (an explicit derivation is shown in appendix A):

$$H' \approx \hbar\omega_0 \sum_{i=1}^{2} a_i^\dagger a_i + \frac{\hbar}{2}\left[\omega_q + \sum_{i=1}^{2}\frac{2g_i^2}{\Delta}\left(a_i^\dagger a_i + \frac{1}{2}\right)\right]\sigma_z + \left(J_0 + \frac{g_1 g_2}{\Delta}\right)(a_1^\dagger a_2 + a_1 a_2^\dagger). \tag{4.3}$$

The second term can be identified as the AC-Stark shifts from photons in each cavity and the third term however contains the cavity-cavity coupling of interest. Whereas in the initial Hamiltonian (4.1) only a direct coupling J_0 occured, the effective Hamiltonian in the dispersive regime (4.3) contains an additional qubit-mediated cavity-cavity coupling rate. For realizing the two-level system with a transmon qubit described in section 2.2, the coupling rates are

$$\hbar g_i \approx 2e\beta_i\omega_i\sqrt{\frac{\hbar Z_0}{\pi}}\left(\frac{E_J}{8E_C}\right)^{1/4}. \tag{4.4}$$

If the flux ϕ through the transmon SQUID loop changes, the Josephson energy E_J and detuning Δ also change according to equations (2.2) and (2.7), respectively. Hence, for the transmon in its ground state ($\sigma_z = -1$), we can tune the total coupling

$$J = J_0 - \frac{g_1 g_2}{\Delta} \tag{4.5}$$

by changing the flux ϕ through the transmon SQUID loop. In the following section, the transmon design is introduced. With electrostatic simulations the individual components of the total coupling J will be estimated for potential applications.

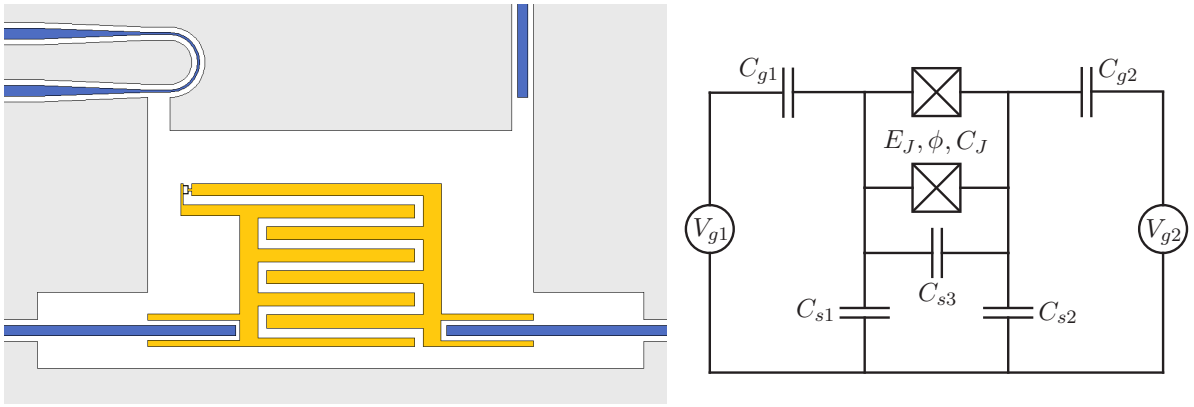

(a) (b)

Figure 4.2: (a) Tunable coupling transmon design coupled to two CPW resonators. (b) Relevant equivalent circuit of the coupling transmon design. The source symbols V_{g1} and V_{g2} indicate the microwave resonators.

4.2 Tunable coupler design

For a first proposal towards a tunable coupling element, I designed a modified transmon qubit as shown in Fig. 4.2 (a) for a resonator mask designed by [Korosec12]. The idea is to couple each qubit electrode tightly to one resonator center-conductor. The resulting equivalent circuit of the effective capacitance network is given in Fig. 4.2 (b). Note that only the most important elements are considered since cross-capacitances are negligible as shown in an electrostatic simulation. The total capacitance which the transmon qubit experiences is given by

$$C_\Sigma = C_s + \frac{(C_{g1} + C_{s1})(C_{g2} + C_{s2})}{C_{g1} + C_{g2} + C_{s1} + C_{s2}}, \tag{4.6}$$

and the capacitance ratios are

$$\beta_i = \frac{C_{gi}(C_{g2} + C_{s2})}{(C_{g1} + C_{s1})(C_{g2} + C_{s2}) + C_s(C_{g1} + C_{g2} + C_{s1} + C_{s2})}, \tag{4.7}$$

for $i = 1, 2$, according to [Johnson11]. The initial transmon design from chapter 3 is modified by larger gaps to keep the island-ground capacitances C_{s1} and C_{s2} small. Also the island-resonator capacitances C_{g1} and C_{g2} significantly increased to get higher coupling rates $g_{1,2}$.

Electrostatic simulation

Based on the design of Fig. 4.2, the individual capacitance elements are obtained by an electrostatic simulation with *Ansoft Maxwell 14*. Since C_{s3} and the Josephson junction capacitance C_J are in parallel, the combination simplifies to $C_s = C_J + C_{s3}$. As in chapter 3, $C_J = 6\,\mathrm{fF}$ is assumed. From the simulated capacitances summarized in Tab. 4.1, the charging energy gets $E_C/h = 165.56\,\mathrm{MHz}$ by evaluating equations (4.6) and (2.4).

Capacitance	Simulated value
C_{s1}	28.89 fF
C_{s2}	30.22 fF
C_{g1}	10.62 fF
C_{g2}	9.83 fF
C_s	97.11 fF

Table 4.1: Capacitance simulation results of the coupling transmon design.

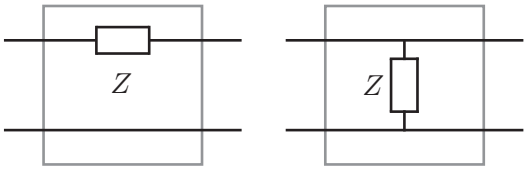

$$\begin{pmatrix} 1 & Z \\ 0 & 1 \end{pmatrix} \qquad \begin{pmatrix} 1 & 0 \\ \frac{1}{Z} & 1 \end{pmatrix}$$

Figure 4.3: Two port network matrices for a series and shunt impedance Z

For an estimation of the resonator-qubit coupling rates, a maximum Josephson energy of $E_{Jmax}/h = 20\,\text{GHz}$ is assumed. The calculations result in $g_1 = 507.46\,\text{MHz}$ and $g_2 = 463.81\,\text{MHz}$.

Direct capacitive coupling

The direct coupling J_0 between the two resonators can be estimated by the capacitance of Fig. 4.2 (b) with an ABCD matrix impedance formalism [Pozar93]. The two-port matrices for an series and shunt impedance are shown in Fig. 4.3. Applying this formalism to the modified transmon design, we get

$$\begin{pmatrix} A & B \\ C & D \end{pmatrix} = \begin{pmatrix} 1 & \frac{1}{i\omega C_{g1}} \\ 0 & 1 \end{pmatrix} \cdot \begin{pmatrix} 1 & 0 \\ 1\omega C_{s1} & 1 \end{pmatrix} \cdot \begin{pmatrix} 1 & \frac{1}{i\omega C_s} \\ 0 & 1 \end{pmatrix} \cdot \begin{pmatrix} 1 & 0 \\ i\omega C_{s2} & 1 \end{pmatrix} \cdot \begin{pmatrix} 1 & \frac{1}{i\omega C_{g2}} \\ 0 & 1 \end{pmatrix} \tag{4.8}$$

The effective coupling capacitance C_{cpl} between the two resonators is obtained by identifying $B \equiv 1/i\omega C_{cpl}$ and algebraic manipulations:

$$C_{cpl} = \frac{C_{g1}C_{g2}C_s}{C_sC_{s1} + C_{g2}(C_s + C_{s1}) + C_sC_{s2} + C_{s1}C_{s2} + C_{g1}(C_{g2} + C_s + C_{s2})} \tag{4.9}$$

By evaluating this equation, a coupling of $C_{cpl} = 1.09\,\text{fF}$ is obtained.

In the next step, the coupling rates J_0 associated with the direct capacitive coupling C_{cpl} is estimated. Two identical resonators, with resonance frequencies $\omega_0/2\pi = 7\,\text{GHz}$, are coupled to an in- and output impedance of $Z_0 = 50\,\Omega$ as shown in Fig. 4.4. The indi-

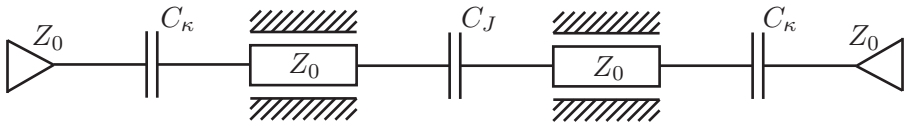

Figure 4.4: Transmission line resonator model of the Dimer. The transmission lines and the input/output ports are matched to $Z_0 = 50\,\Omega$

vidual resonators are modeled by transmission lines of length l, described by coefficients

$$\begin{aligned} t_{11} &= \cosh(i\gamma l), \\ t_{12} &= Z_0 \sinh(i\gamma l), \\ t_{21} &= 1/Z_0 \sinh(i\gamma l), \\ t_{22} &= \cosh(i\gamma l), \end{aligned} \tag{4.10}$$

where $\gamma = \alpha + i\beta$. For simplicity, we consider lossless transmission lines with $\alpha = 0$. The propagation coefficient $\beta l = \omega l / v_{ph}$ can be rewritten by the resonance condition $\omega_0 = \pi v_{ph}/l$ as

$$\beta l = \pi \frac{\omega}{\omega_0}. \tag{4.11}$$

For the coupling capacitances $C_\kappa = 7.48\,\mathrm{fF}$ obtained from [Korosec12], the total ABCD matrix according to Fig. 4.4 reads

$$\begin{pmatrix} A & B \\ C & D \end{pmatrix} = \begin{pmatrix} 1 & \frac{-1}{i\omega C_\kappa} \\ 0 & 1 \end{pmatrix} \cdot \begin{pmatrix} t_{11} & t_{12} \\ t_{21} & t_{22} \end{pmatrix} \cdot \begin{pmatrix} 1 & \frac{-1}{i\omega C_J} \\ 0 & 1 \end{pmatrix} \cdot \begin{pmatrix} t_{11} & t_{12} \\ t_{21} & t_{22} \end{pmatrix} \cdot \begin{pmatrix} 1 & \frac{-1}{i\omega C_\kappa} \\ 0 & 1 \end{pmatrix} \tag{4.12}$$

With the ABCD matrix model, the transmission spectrum is given by

$$S_{21} = 10 \log \left| \frac{2}{A + B/Z_0 + CZ_0 + D} \right| \mathrm{dB} \tag{4.13}$$

Fig. 4.5 shows the transmission spectrum S_{21} as a function of $\omega/2\pi$. The separation of the two peaks is equal to $2J_0$ [Karalic13]. Thus, the estimated coupling energy due to the direct capacitive couplingC_{cpl} is $J_0/2\pi = 5.26\,\mathrm{MHz}$.

4.3 Tunable coupling analysis

In this last section, I will discuss the tunability of the total coupling based on the electrostatic simulations above. The total coupling J from the transformed Hamiltonian of equation (4.3) is given by

$$J = J_0 - \frac{g_1 g_2}{\Delta}, \tag{4.14}$$

if the transmon qubit is in the ground state, i.e. $\sigma_z = -1$. Fig. 4.6 shows a plot of the total coupling as a function of the flux ϕ through the transmon SQUID loop. Note

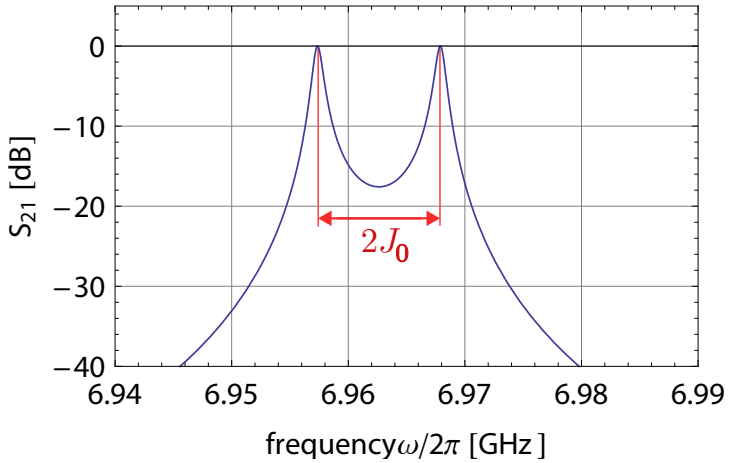

Figure 4.5: Transmission spectrum S_{21} of the Dimer array according to Fig. 4.4. The distance between the two peaks is given by $2J_0$

that at $\phi \sim 0.5\,\phi_0/\pi$ the total transmission is zero. This turn off point has interesting applications discussed below. Moreover, the qubit dispersions $g_{1,2}/\Delta \ll 1$ should hold in order to justify the SW transformation of section 4.1. In Fig. 4.6 (b), the qubit dispersion is given dependent on the flux ϕ. The dispersive regime $g_{1,2}/\Delta \ll 1$ is only reached above $\phi > 0.34\,\phi_0/\pi$. In fact, this could yield to problems for high coupling rates J since higher order processes are in (4.3) are not suppressed substantially. In conclusion, the low order approximation for the tunable coupling works only for $0 \ll J/2\pi \ll 40\,\mathrm{MHz}$.

The main application of the tunable coupling element is changing the g/J ratio for a cavity array *in-situ*. Further possible applications of such a tunable coupling element described in this chapter include cavity switches [Mariantoni08] and new qubit readout schemes, where the coupling is adjusted dynamically [Sete13].

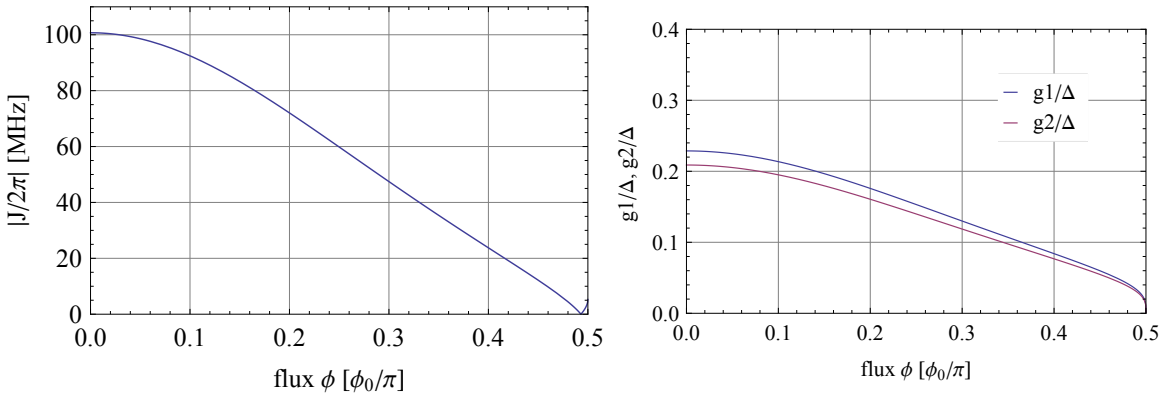

Figure 4.6: (a) Total resonator-resonator coupling $|J|$ and (b) resonator-qubit dispersion dependent on the flux ϕ through the SQUID loop.

Conclusion

In summary, the purpose of this thesis was to design a transmon qubit for cavity arrays in circuit QED. After a short motivation for quantum simulation with cavity QED systems and a brief introduction to circuit QED theory, the transmon design properties were investigated with electrostatic simulations. Moreover, in the new design I attempt to improve qubit coherence times by increasing the gaps between the individual superconducting elements. Based on the design, a Dimer sample was fabricated. The last part in this thesis focused on a *in-situ* tunable resonator-resonator coupling element, where a two-level system inbetween two resonators can mediate a dispersive coupling. A first approach towards an implementation by using a modified transmon qubit as a two-level system was discussed. The realization of a tunable coupling would allow to interesting applications such as cavity switches and new qubit readout schemes.

Outlook: Majorana-like modes

In addition to the quantum simulation models introduced in the beginning, I would like to outlook a recent theoretical proposal suggested the observation of Majorana-like modes of light in a circuit QED cavity array [Bardyn12]. The starting point is a Bose-Hubbard model which we can achieve with a cavity array in the strong coupling regime of the individual resonator-qubit systems. In order to observe exotic non-Abelian properties, a additional parametric drive element H_{drive} to achieve a p-wave pairing is required:

$$H_{drive} = -|\Delta| \sum_{i=1}^{N-1} \left(e^{i(2\omega_p t + \phi)} \hat{a}_i \hat{a}_{i+1} + h.c. \right), \tag{4.15}$$

where $|\Delta| e^{i\phi}$ denotes a coherent pump drive with a frequency ω_p. Recent proposals suggested possible implementation schemes by embedding Josephson junctions or SQUID loops inbetween coplanar microwave resonators [Peropadre13]. In conclusion, once a parametric drive element is realized, the observation of such exotic particle statistics would open new possibilities.

Acknowledgments

I would like to thank Prof. Andreas Wallraff for giving me the opportunity to work on this semester thesis. Moreover, I am deepley grateful to Milan Allan for supervising and inspiring my work. I appreciate the valuable discussions with Christohper Eichler and thank all members of the Quantum Device Lab at ETH Zurich for the pleasant atmosphere.

Bibliography

[Bardyn12] C.-E. Bardyn, M. A. Baranov, E. Rico, A. İmamoğlu, P. Zoller, and S. Diehl. "Majorana modes in driven-dissipative atomic superfluids with a zero chern number." *Phys. Rev. Lett.*, **109**, 130402 (2012).

[Barreiro11] J. T. Barreiro, M. Muller, P. Schindler, D. Nigg, T. Monz, M. Chwalla, M. Hennrich, C. F. Roos, P. Zoller, and R. Blatt. "An open-system quantum simulator with trapped ions." *Nature*, **470**, 486–491 (2011).

[Blais04] A. Blais, R.-S. Huang, A. Wallraff, S. M. Girvin, and R. J. Schoelkopf. "Cavity quantum electrodynamics for superconducting electrical circuits: An architecture for quantum computation." *Physical Review A*, **69**, 062320 (2004).

[Bravy11] S. Bravy, D. P. DiVincenzo, and D. Loss. "Schrieffer-wolff transformation for quantum many-body systems." *arXiv:1105.0675* (2011).

[Burkhard12] S. Burkhard. "Optimization of transmon design for long coherence time." Semester thesis, ETH Zurich (2012).

[Chang13] J. Chang, M. R. Vissers, A. D. Corcoles, M. Sandberg, J. Gao, D. W. Abraham, J. M. Chow, J. M. Gambetta, M. B. Rothwell, G. A. Keefe, M. Steffen, and D. P. Pappas. "Improved superconducting qubit coherence using titanium nitride." *arXiv:1303.4071* (2013).

[Chow12] J. M. Chow, J. M. Gambetta, A. D. Córcoles, S. T. Merkel, J. A. Smolin, C. Rigetti, S. Poletto, G. A. Keefe, M. B. Rothwell, J. R. Rozen, M. B. Ketchen, and M. Steffen. "Universal quantum gate set approaching fault-tolerant thresholds with superconducting qubits." *Phys. Rev. Lett.*, **109**, 060501 (2012).

[Correa13] B. V. Correa, A. Kurcz, and J. j. Garcia-Ripoll. "Bose-hubbard models with photon pairing in circuit-qed." *arXiv:1304.7196* (2013).

[Devoret97] M. H. Devoret. "Quantum fluctuations in electrical circuits." In S. Reynaud, E. Giacobino, and J. Zinn-Justin, editors, "Quantum Fluctuations: Les Houches Session LXIII," 351–386. Elsevier (1997).

[Devoret04a] M. H. Devoret and J. M. Martinis. "Implementing qubits with superconducting integrated circuits." *Quantum Information Processing*, **3**, 163–203 (2004).

[Devoret04b] M. H. Devoret, A. Wallraff, and J. M. Martinis. "Superconducting qubits: A short review." *cond-mat/0411174* (2004).

[Devoret07] M. Devoret, S. Girvin, and R. Schoelkopf. "Circuit-QED: How strong can the coupling between a Josephson junction atom and a transmission line resonator be?" *Annalen der Physik*, **16**, 767–779 (2007).

[Dimitris10] I. Dimitris, S. Ashhab, and F. Nori. "Using superconducting qubit circuits to engineer exotic lattice systems." *Phys. Rev. A*, **82**, 052311 (2010).

[Feynman82] R. P. Feynman. "Simulating physics with computers." *Int. J. Theor. Phys.*, **21**, 467–488 (1982).

[Fink10] J. Fink. *Quantum nonlinearities in strong coupling circuit QED.* Ph.D. thesis, ETH Zurich (2010).

[Fisher89] M. P. A. Fisher, P. B. Weichman, G. Grinstein, and D. S. Fisher. "Boson localization and the superfluid-insulator transition." *Phys. Rev. B*, **40**, 546–570 (1989).

[Gersch62] H. A. Gersch and G. C. Knollman. "Quantum cell model for bosons." *Phys. Rev.*, **129**, 959–967 (1962).

[Gevorgian95] S. Gevorgian, L. J. P. Linnér, and E. L. Kollberg. "CAD models for shielded multilayered CPW." *IEEE T. Microw. Theory.*, **43(2)**, 772 (1995).

[Girvin09] S. M. Girvin, M. H. Devoret, and R. J. Schoelkopf. "Circuit qed and engineering charge-based superconducting qubits." *Phys. Scr.*, **2009**, 014012 (2009).

[Göppl08] M. Göppl, A. Fragner, M. Baur, R. Bianchetti, S. Filipp, J. M. Fink, P. J. Leek, G. Puebla, L. Steffen, and A. Wallraff. "Coplanar waveguide resonators for circuit quantum electrodynamics." *Journal of Applied Physics*, **104**, 113904 (2008).

[Göppl09] M. Göppl. *Engineering Quantum Electronic Chips - Realization and Characterization of Circuit Quantum Electrodynamics Systems.* Ph.D. thesis, ETH Zurich (2009).

[Govenius12] J. Govenius. *Single-Shot Qubit Readout in Circuit QED using Parametric Amplification.* Master's thesis, ETH Zurich (2012).

[Greentree06] A. D. Greentree, C. Tahan, J. H. Cole, and L. C. L. Hollenberg. "Quantum phase transitions of light." *Nat. Phys.*, **2**, 856–861 (2006).

[Greiner02] M. Greiner, O. Mandel, T. Esslinger, T. W. Hansch, and I. Bloch. "Quantum phase transition from a superfluid to a mott insulator in a gas of ultracold atoms." *Nature*, **415**, 39–44 (2002).

[Hartmann06] M. J. Hartmann, F. G. S. L. Brandao, and M. B. Plenio. "Strongly interacting polaritons in coupled arrays of cavities." *Nat Phys*, **2**, 849–855 (2006).

[Hartmann08] M. Hartmann, F. Brandao, and M. Plenio. "Quantum many-body phenomena in coupled cavity arrays." *Laser & Photon. Rev.*, **2**, 527–556 (2008).

[Houck12] A. A. Houck, H. E. Tureci, and J. Koch. "On-chip quantum simulation with superconducting circuits." *Nat. Phys.*, **8**, 292–299 (2012).

[Hubbard63] J. Hubbard. "Electron correlations in narrow energy bands." *Proc. R. Soc. (London) A*, **276, no. 1365**, 238–257 (1963).

[Imamoğlu97] A. Imamoğlu, H. Schmidt, G. Woods, and M. Deutsch. "Strongly interacting photons in a nonlinear cavity." *Phys. Rev. Lett.*, **79**, 1467–1470 (1997).

[Ithier05] G. Ithier, E. Collin, P. Joyez, P. J. Meeson, D. Vion, D. Esteve, F. Chiarello, A. Shnirman, Y. Makhlin, J. Schriefl, and G. Schön. "Decoherence in a superconducting quantum bit circuit." *Phys. Rev. B*, **72**, 134519 (2005).

[Jaynes63] E. Jaynes and F. Cummings. "Comparison of quantum and semiclassical radiation theories with application to the beam maser." *Proceedings of the IEEE*, **51**, 89–109 (1963).

[Johnson11] B. Johnson. *Controlling Photons in Superconducting Electrical Circuits.* Ph.D. thesis, Yale (2011).

[Josephson62] B. D. Josephson. "Possible new effects in superconductive tunnelling." *Physics Letters*, **1**, 251–253 (1962).

[Karalic13] M. Karalic. "Characterization of coupled microwave resonator arrays, to be published." Semester thesis, ETH Zurich (2013).

[Koch07] J. Koch, T. M. Yu, J. Gambetta, A. A. Houck, D. I. Schuster, J. Majer, A. Blais, M. H. Devoret, S. M. Girvin, and R. J. Schoelkopf. "Charge-insensitive qubit design derived from the Cooper pair box." *Phys. Rev. A*, **76**, 042319 (2007).

[Korosec12] L. Korosec. "Design of nonlinear resonator arrays in superconducting circuits." Semester thesis, ETH Zurich (2012).

[Lang11] C. Lang, D. Bozyigit, C. Eichler, L. Steffen, J. M. Fink, A. A. Abdumalikov Jr., M. Baur, S. Filipp, M. P. da Silva, A. Blais, and A. Wallraff. "Observation of resonant photon blockade at microwave frequencies using correlation function measurements." *Phys. Rev. Lett.*, **106**, 243601 (2011).

[Leib10] M. Leib and M. Hartmann. "Bose hubbard dynamics of polaritons in a chain of circuit quantum electrodynamics cavities." *New J. Phys.*, **12**, 093031 (2010).

[Makhlin01] Y. Makhlin, G. Schön, and A. Shnirman. "Quantum-state engineering with Josephson-junction devices." *Rev. Mod. Phys.*, **73**, 357–400 (2001).

[Mariantoni08] M. Mariantoni, F. deppe, A. Marx, R. Gross, F. K. Wilhelm, and E. Solano. "Two-resonator circuit quantum electrodynamics: A superconducting quantum switch." *Phys. Rev. B*, **78**, 104508 (2008).

[Nakamura99] Y. Nakamura, Y. A. Pashkin, and J. S. Tsai. "Coherent control of macroscopic quantum states in a single-Cooper-pair box." *Nature*, **398**, 786–788 (1999).

[Nissen12] F. Nissen, S. Schmidt, M. Biondi, G. Blatter, H. E. Tureci, and J. Keeling. "Non-equilibrium dynamics of coupled qubit-cavity arrays." *Phys. Rev. Lett.*, **108**, 233603 (2012).

[Peropadre13] B. Peropadre, D. Zueco, F. Wulschner, F. Deppe, A. Marx, R. Gross, and J. J. García-Ripoll. "Tunable coupling engineering between superconducting resonators: From sidebands to effective gauge fields." *Phys. Rev. B*, **87**, 134504– (2013).

[Plenio04] M. B. Plenio, J. Hartley, and J. Eisert. "Dynamics and manipulation of entanglement in coupled harmonic systems with many degrees of freedom." *New. J. Phys.*, **6**, 36 (2004).

[Pozar93] D. M. Pozar. *Microwave Engineering.* Addison-Wesley Publishing Company (1993).

[Romero-Isart07] O. Romero-Isart, K. Eckert, R. C., and A. Sanpera. "Transport and entanglement generation in the bose-hubbard model." *Journal of Physics A: Mathematical and Theoretical*, **40**, 8019 (2007).

[Schmidlin08] S. Schmidlin. *Design and characterization of microwave Printed Circuit Boards for circuit QED experiments.* Master's thesis, ETH Zurich (2008).

[Schmidt09] S. Schmidt and G. Blatter. "Strong coupling theory for the jaynes-cummings-hubbard model." *Phys. Rev. Lett.*, **103**, 086403 (2009).

[Schmidt12] S. Schmidt and J. Koch. "Circuit qed lattices: towards quantum simulation with superconducting circuits." *arXiv:1212.2070* (2012).

[Sete13] E. A. Sete, A. Galiautdinov, E. Mlinar, J. M. Martinis, and A. N. Korotkov. "Catch-disperse-release readout for superconducting qubits." *Phys. Rev. Lett.*, **110**, 210501– (2013).

[Steffen13] L. Steffen, A. Fedorov, M. Oppliger, Y. Salathe, P. Kurpiers, M. Baur, G. Puebla-Hellmann, C. Eichler, and A. Wallraff. "Realization of deterministic quantum teleportation with solid state qubits." *arXiv:1302.5621* (2013).

[Van Duzer81] T. Van Duzer and C. Turner. *Principles of superconducting devices and circuits.* Edward Arnold, U.K. (1981).

[Wallraff04] A. Wallraff, D. I. Schuster, A. Blais, L. Frunzio, R.-S. Huang, J. Majer, S. Kumar, S. M. Girvin, and R. J. Schoelkopf. "Strong coupling of a single photon to a superconducting qubit using circuit quantum electrodynamics." *Nature*, **431**, 162–167 (2004).

[Walls94] D. F. Walls and G. J. Milburn. *Quantum Optics.* Springer Verlag, Berlin (1994).

[Walther06] H. Walther, B. T. H. Varcoe, B.-G. Englert, and T. Becker. "Cavity quantum electrodynamics." *Reports on Progress in Physics*, **69**, 1325–1382 (2006).

[Yamamoto99] Y. Yamamoto and A. Imamoğlu. *Mesoscopic Quantum Optics.* Wiley (1999).

[Zohar13] E. Zohar, J. Cirac, and B. Reznik. "Quantum simulations of gauge theories with ultracold atoms: local gauge invariance from angular momentum conservation." *arXiv.org*, **1303.5040** (2013).

Appendix A

Two-cavity architecture Hamiltonian

The derivation of the effective two-cavity architecture Hamiltonian described in section section 4.1 involves commutator algebra. In the first section I will give an overview of the most important steps concerning the Schrieffer-Wolff transformation. Section two shows how to make such a transformation using the *Mathematica* Add-on by José Luis Gómez-Munõz and Francisco Delgado.

A.1 Schrieffer-Wolff transformation

The bosonic commutation relations for the creation (annihilation) operator $\hat{a}_i^\dagger$ ($\hat{a}_i$) describing the cavity fields are

$$[\hat{a}_i^\dagger \hat{a}_i, \hat{a}_j] = -\delta_{ij}\hat{a}_j, \qquad \text{and} \qquad [\hat{a}_i^\dagger \hat{a}_i, \hat{a}_j^\dagger] = \delta_{ij}\hat{a}_j^\dagger. \tag{A.1}$$

The two-level system is represented by the Pauli Spin 1/2 notation

$$[\hat{\sigma}_z, \hat{\sigma}^\pm] = \pm 2\hat{\sigma}^\pm, \qquad \text{and} \qquad [\hat{\sigma}^+, \hat{\sigma}^-] = \hat{\sigma}_z, \tag{A.2}$$

where $\hat{\sigma}^\pm \equiv (\hat{\sigma}_x \pm i\hat{\sigma}_y)/2$. A new operator $\hat{X}_i$ defined by

$$\hat{X}_i \equiv \hat{a}_i\hat{\sigma}^+ + \hat{a}_i^\dagger\hat{\sigma}^-, \tag{A.3}$$

will simplify further calculations. The Jaynes-Cummings Hamiltonian H for the two-cavity architecture as explained in section 4.1 is

$$H = \sum_{i=1}^{2} \hbar\omega_i \hat{a}_i^\dagger \hat{a}_i + \frac{\hbar}{2}\omega_q\hat{\sigma}_z + \sum_{i=1}^{2} \hbar g_i \left(\hat{a}_i\hat{\sigma}^+ - \hat{a}_i^\dagger\hat{\sigma}^-\right). \tag{A.4}$$

By using the unitary transformation

$$U = e^{\sum_i \frac{g_i}{\Delta_i}\hat{X}_i}, \tag{A.5}$$

and the Barker-Campbell-Hausdorff relation

$$e^{\hat{X}}\hat{Y}e^{-\hat{X}} = \hat{Y} + [\hat{X},\hat{Y}] + \frac{1}{2}\left[\hat{X},[\hat{X},\hat{Y}]\right] + ... \,, \tag{A.6}$$

it is possible to express $H' = UHU^\dagger$ by

$$\begin{aligned} H' \approx H + \sum_{i,j=1}^{2} \hbar\omega_i \frac{g_j}{\Delta_j}\left[\hat{X}_j, \hat{a}_i^\dagger \hat{a}_i\right] + \frac{1}{2}\sum_{i,j,k=1}^{2} \hbar\omega_i \frac{g_k g_j}{\Delta_k \Delta_j}\left[\hat{X}_k, \left[\hat{X}_j, \hat{a}_i^\dagger \hat{a}_i\right]\right] \\ + \frac{\hbar}{4}\omega_q \sum_{j=1}^{2} \frac{g_j}{\Delta_j}\left[\hat{X}_i, \hat{\sigma}_z\right] + \frac{\hbar}{2}\omega_q \sum_{i,j=1}^{2} \frac{g_i g_j}{\Delta_i \Delta_j}\left[\hat{X}_j, \left[\hat{X}_i, \hat{\sigma}_z\right]\right] + \sum_{i,j=1}^{2} \hbar g_i \frac{g_j}{\Delta_j}\left[\hat{X}_j, \hat{X}_i\right], \end{aligned} \tag{A.7}$$

where terms of higher order than g_i^2/Δ_i^2 are neglected. The most important commutation relations between $\hat{a}_i^\dagger \hat{a}_i$, $\hat{\sigma}_z$ and $\hat{X}_i$ in H' are given by

$$[\hat{X}_j, \hat{a}_i^\dagger \hat{a}_i] = \frac{1}{2}\delta_{ij}\left(\hat{a}_i \hat{\sigma}^+ - \hat{a}_i^\dagger \hat{\sigma}^-\right), \tag{A.8}$$

$$[\hat{X}_i, \hat{\sigma}_z] = -\hat{a}_i \hat{\sigma}^+ + \hat{a}_i^\dagger \hat{\sigma}^-, \tag{A.9}$$

$$[\hat{X}_j, \hat{X}_i] = \left(\hat{a}_i^\dagger \hat{a}_j - \hat{a}_j^\dagger \hat{a}_i\right)\hat{\sigma}_z, \tag{A.10}$$

$$\left[\hat{X}_k, [\hat{X}_j, \hat{a}_i^\dagger \hat{a}_i]\right] = -\delta_{ij}\left(\delta_{ik}\left(\mathbb{1} - \hat{\sigma}_z\right) + \hat{a}_i^\dagger \hat{a}_k \hat{\sigma}_z + \hat{a}_k^\dagger \hat{a}_i \hat{\sigma}_z\right), \tag{A.11}$$

$$\left[\hat{X}_j, [\hat{X}_i, \hat{\sigma}_z]\right] = 2\delta_{ij}\left(\mathbb{1} - \hat{\sigma}_z\right) + \hat{a}_i^\dagger \hat{a}_j \hat{\sigma}_z + \hat{a}_j^\dagger \hat{a}_i \hat{\sigma}_z. \tag{A.12}$$

By using the relations (A.8) to (A.12), various terms cancel and the result reads

$$H' \approx \sum_{i=1}^{2} \hbar\omega_i \hat{a}_i^\dagger \hat{a}_i + \frac{\hbar}{2}\left(\omega_q + \sum_{i=1}^{2} \frac{g_i^2}{\Delta_i} + \sum_{i=1}^{2} \frac{2g_i^2}{\Delta_i}\hat{a}_i^\dagger \hat{a}_i\right)\hat{\sigma}_z + \frac{2g_1 g_2(\Delta_1 + \Delta_2)}{\Delta_1 \Delta_2}(\hat{a}_1^\dagger \hat{a}_2 + \hat{a}_1 \hat{a}_2^\dagger). \tag{A.13}$$

For two cavities with same resonance frequencies $\omega_1 = \omega_2 \equiv \omega_0$, the effective Hamiltonian H' reduces to

$$H' \approx \hbar\omega_0 \sum_{i=1}^{2} \hat{a}_i^\dagger \hat{a}_i + \frac{\hbar}{2}\left[\omega_q + \sum_{i=1}^{2} \frac{2g_i^2}{\Delta}\left(\hat{a}_i^\dagger \hat{a}_i + \frac{1}{2}\right)\right]\hat{\sigma}_z + \frac{g_1 g_2}{\Delta}(\hat{a}_1^\dagger \hat{a}_2 + \hat{a}_1 \hat{a}_2^\dagger). \tag{A.14}$$

A.2 Commutator Algebra with Mathematica

The derivation of the two cavity Hamiltonian with the Schrieffer-Wolff transformation described above is rather intense, even for simple configurations. Therefore, a *Mathematica* Add-on from José Luis Gómez-Munõz and Francisco Delgado is useful to simplify the commutation relations. The packages and instructions can be found at "http://homepage.cem.itesm.mx/lgomez/quantum/".

(*Initialization routine*)

Needs[“QuantumNotation”];

SetQuantumAliases[];

(*Field operator definitions*)

SetQuantumObject[$a, \hat{\sigma}$];

$[[a_{i\_}, a_{j\_}{}^{\dagger}]]_{\_}$:=KroneckerDelta[$i, j$];

$[[a_{i\_}, a_{j\_}]]_{\_}$:=0; $[[a_{i\_}{}^{\dagger}, a_{j\_}{}^{\dagger}]]_{\_}$:=0;

(*Pauli Algebra definitions*)

$\hat{\sigma}_{a:0|1|2|3}{}^{2}$:=$\hat{\sigma}_0$;

$\hat{\sigma}_{a:0|1|2|3}{}^{\dagger}$:=$\hat{\sigma}_a$;

$\hat{\sigma}_{a:0|1|2|3} \cdot \hat{\sigma}_0$:=$\hat{\sigma}_a$;

$\hat{\sigma}_0 \cdot \hat{\sigma}_{b:0|1|2|3}$:=$\hat{\sigma}_b$;

$\hat{\sigma}_{a:1|2|3} \cdot \hat{\sigma}_{b:1|2|3}$:=KroneckerDelta$[a, b] * \hat{\sigma}_0 + i * \sum_{c=1}^{3}$ Signature$[\{a, b, c\}] * \hat{\sigma}_c$;

$[[\hat{\sigma}_0, \hat{\sigma}_{b:0|1|2|3}]]_{\_}$:=0;

$[[\hat{\sigma}_{a:1|2|3}, \hat{\sigma}_{b:1|2|3}]]_{\_}$:=$2 * i * \sum_{c=1}^{3}$ Signature$[\{a, b, c\}] * \hat{\sigma}_c$;

$[[\hat{\sigma}_0, \hat{\sigma}_{b:0|1|2|3}]]_{+}$:=$2 * \hat{\sigma}_b$;

$[[\hat{\sigma}_{a:1|2|3}, \hat{\sigma}_{b:1|2|3}]]_{+}$:=$2 *$ KroneckerDelta$[a, b] * \hat{\sigma}_0$;

$\hat{\sigma}^{+}$:=$\frac{1}{2}(\hat{\sigma}_1 + i\hat{\sigma}_2)$;

$\hat{\sigma}^{-}$:=$\frac{1}{2}(\hat{\sigma}_1 - i\hat{\sigma}_2)$;

$[[\hat{\sigma}_{b:1|2|3}, a_{i\_}]]_{\_}$:=0;

$[[\hat{\sigma}_{b:1|2|3}, a_{i\_}{}^{\dagger}]]_{\_}$:=0;

$[[a_{i\_}, \hat{\sigma}_{b:1|2|3}]]_{\_}$:=0;

$[[a_{i\_}{}^{\dagger}, \hat{\sigma}_{b:1|2|3}]]_{\_}$:=0;

After the initialization, define the system Hamiltonian H and the unitary operator X.

Clear$[H, X]$

$H = \sum_{i=1}^{2} \hbar\omega_i {a_i}^\dagger \cdot a_i + \frac{\hbar}{2}\omega_q \hat{\sigma}_3 + \sum_{i=1}^{2} \hbar g_i \left(a_i \cdot \hat{\sigma}^+ + {a_i}^\dagger \cdot \hat{\sigma}^-\right);$

$X = \sum_{i=1}^{2} \frac{g_i}{\Delta_i} \left(a_i \cdot \hat{\sigma}^+ + {a_i}^\dagger \cdot \hat{\sigma}^-\right);$

In the next step, the Barker-Campbell-Hausdorff relation for H' is evaluated for the coupling between the two cavities, i.e. terms which exploit $(a_1^\dagger a_2 + a_2^\dagger a_1)$. The resulting cavity-cavity coupling term equals the result of section A.1 and [Johnson11] for $\Delta_{1,2} = \omega_q - \omega_{1,2}$.

Simplify[1/2Total[Simplify $\left[\text{Total}/@\text{Coefficient}\left[H + [[X, H]]_- + \frac{1}{2}[[X, [[X, H]]_-]]_-\right.\right.$,

$\left.\left.\text{Permutations}/@\left\{{a_1}^\dagger \cdot a_2 \cdot \hat{\sigma}_3, {a_2}^\dagger \cdot a_1 \cdot \hat{\sigma}_3\right\}\right]\right]]$

$-\frac{\hbar g_1 g_2 (\omega_1 + \omega_2 - 2\omega_q)}{2\Delta_1 \Delta_2}$

Appendix B

Project file directory

The folders explained in the following contain the relevant project files which can be found at "Q:\USERS\Lukas_Heinzle\dimer_thesis\". Note that sub-folders called "_dev\" contain old backup files.

Folder	Contents
_lukas_korosec_data	Database and documentation for the M25 resonator mask design [Korosec12].
calculations	Miscellaneous *Mathematica* files, where "two_cavity_Hamiltonian.nb" contains the calculation of appendix A.2.
Mask25_ebeam	Electron beam lithography files for sample fabrication.
Maxwell	Electrostatic simulation files for the transmon design ("mask25_cavity_transmon") and the tunable coupler proposal ("mask25_tunable_transmon"). The AutoCAD design files for sample fabrication are also included.
misc	Miscellaneous *HFSS* and *Microwave office* simulation files.
papers	Relevant articles, papers and theses.
pics	Figures, images and graphs.
talks	Quantum Device Lab Group seminar talk about "Towards quantum simulation with coupled cavity arrays".
thesis	"v5_corr" contains the actual semester thesis documentation.